Journal of *Marine Science and Engineering*

MDPI

Article

The Effect of Multiple Factors on the Fatigue Crack Growth Behavior of DH36 Steel in Arctic Environment

Kaiqing Qiao [1,2], Zhijie Liu [1,2,*], Zhenyu Sun [1,2], Qiuyu Guo [1,2] and Xiaobang Wang [1,2]

[1] Naval Architecture and Ocean Engineering College, Dalian Maritime University, Dalian 116026, China; qkq15840342308@163.com (K.Q.); 15524159717@163.com (Z.S.); guoqiuyu1016@163.com (Q.G.); wxb@dlmu.edu.cn (X.W.)

[2] Key Laboratory for Polar Safety Assurance Technology and Equipment of Liaoning Province, Dalian 116026, China

* Correspondence: liuzj@dlmu.edu.cn

Abstract: In Arctic regions, ship structures face low temperatures, overloads, thickness effects, and fluctuating stress ratios, which significantly influence the fatigue crack growth (FCG) behavior of marine steels. This study investigates the FCG behaviors of DH36 steel by a series of experiments under the combined effects of low temperatures, overload ratios R_{ol}, specimen thickness B, and stress ratios R. Experiment results show that the yield strength, ultimate tensile strength, and elastic modulus of DH36 steel exhibit negative correlations with temperature varying within the Arctic temperature range. A reduction in fatigue crack growth rate (FCGR) is observed under the combined effects of low temperature and overload, and the magnitude of decrease shows a positive correlation with R_{ol}. Notably, low temperatures weaken the FCG retardation effect induced by overload, and this attenuation becomes more pronounced as temperature decreases. Under low temperatures, while maintaining constant peak load, increasing R significantly reduces both initial and terminal stress intensity factor ranges ΔK_0 and ΔK_e, resulting in diminished effective crack driving force and thereby substantially extending FCG life. Although increased B enhances FCGR at low temperatures, thinner plates demonstrate shorter FCG life due to their higher ΔK_0 values.

Keywords: low temperature; DH36 steel; fatigue crack growth behavior; stress ratio; overload ratio; thickness effect

check for updates

Academic Editor: Weicheng Cui

Received: 8 May 2025
Revised: 25 May 2025
Accepted: 31 May 2025
Published: 3 June 2025

Citation: Qiao, K.; Liu, Z.; Sun, Z.; Guo, Q.; Wang, X. The Effect of Multiple Factors on the Fatigue Crack Growth Behavior of DH36 Steel in Arctic Environment. *J. Mar. Sci. Eng.* **2025**, *13*, 1118. https://doi.org/10.3390/jmse13061118

Copyright: © 2025 by the authors. Licensee MDPI, Basel, Switzerland. This article is an open access article distributed under the terms and conditions of the Creative Commons Attribution (CC BY) license (https://creativecommons.org/licenses/by/4.0/).

1. Introduction

Despite the Arctic's abundance of natural resources, its extreme environments, such as severe cold, ice accumulation, and strong winds, pose serious challenges to the fatigue performance of polar ship structures [1,2]. According to a Lloyd's Register survey of 690 ice-class vessels, 57% of hulls develop visible cracks or fractures by an average service age of 13 years, with 38% of these defects concentrated in the bow region. The fatigue life is significantly shorter than that of conventional sea vessels [3]. Therefore, under the combined effect of low temperature and complex loads as well as size effect, the fatigue performance of marine steel becomes a key factor to ensure the operational safety and structural integrity of polar ship equipment [4,5].

Fatigue analysis of ship structures primarily involves two approaches: the stress-life (*S-N*) curve technique [6,7] and the fracture mechanics-based approach [8,9]. Among them, the *S-N* curve technique is widely applied during the structural design phase of hulls; whereas, once a crack is detected in service, the fatigue crack growth (FCG) life is evaluated

by the fracture mechanics method to develop a reasonable repair plan and inspection cycle. Some scholars have used fracture mechanics to systematically investigate the fatigue crack growth (FCG) behavior of marine steel from various perspectives, such as low temperature, stress ratio, overload ratio, weld residual stress, and microstructure, in response to the limited rescue and repair conditions faced by ship structures in Arctic service [10].

Igwemezie et al. [11] examined the effect of microstructural FCG character in marine-grade S355 steel, and the results showed that crack deflection, crack bifurcation, and metal debris formation are the main factors that retard the crack growth of steel, which are jointly influenced by the material microstructure, service environment, and crack tip state. Shen et al. [12] investigated the impacts of varying stress ratios R on the FCG character of EH690 base metal and its welded joints. The results showed that the heat-affected zone and the weld metal exhibited higher cracking resistance compared to the base material and that higher stress ratios accelerated the FCGR of the EH690 base material and welded joints. Wang et al. [13] analyzed the FCG character of marine steel AH36 under variable amplitude loading and showed that the FCG life of AH36 steel increased significantly with increasing overload ratio R_{ol} and that the greater the crack tip strain accumulation, the more significant the retardation effect produced by overload. Zhao et al. [14] investigated the effect of low temperature on the FCGR of marine steel DH36 and its butt welds, and the results showed that the FCGR of both the base metal and butt welds of DH36 decreased to different degrees with the decrease of test temperature. Compared to room temperature, -60 °C led to higher Vickers hardness in both the base material and the welds. Moreover, the welds maintained greater hardness than the base in both temperature conditions. Tu et al. [15] researched the FCG behavior of marine steel AH36 with respect to different loads and proposed an extended finite element method for calculating the plastic zone dimension adjacent to the crack tip. The results show that with the increase of R_{ol}, overload leads to a more significant retardation effect, but underloading after overloading weakens the effect. Qin et al. [16] analyzed the effect of peak load F_{max} versus R on FCGR of marine steel, and the results showed that crack tip opening displacement (CTOD) increases as F_{max} becomes larger at constant R, and at constant F_{max}, the CTOD decreased significantly with increasing R. In addition, significant plastic deformation accumulation occurs at the crack tip with the increase in the number of loading cycles, which has an effect on FCGR and CTOD. Li et al. [17] performed an experimental investigation of the FCG behavior of marine steel 925A at low temperatures, and the results showed that temperature reduction significantly extended the FCG life of 925A steel. Based on scanning electron microscopy (SEM) observations, there are obvious cleavage fracture characteristics in the stable growth zone at -60 °C. Song et al. [18] performed an experimental investigation of the FCG performance of marine steel D32 and its overmatched welded joints at different R. The findings revealed that welding-induced residual stresses led to a reduced FCGR in both the heat-affected zone (HAZ) and the fusion zone. The findings indicated that the residual stresses in the welded joints reduced the FCGR in the heat-affected and fusion zones, which prolonged the FCG life. Wang et al. [19] analyzed the FCG behavior of EH36 steel under Arctic low temperature conditions. Their results demonstrated that the FCGR was significantly reduced compared to that observed at room temperature, and the FCGR threshold value increased as the temperature decreased.

Thickness of marine steel has a significant impact on equipment energy consumption and plays a key role in achieving green navigation [20]. However, studies on the thickness influences on the FCG behavior of marine steels are scarce and mostly limited to ambient conditions. Park et al. [21] investigated the effect of specimen thickness B on the FCGR of 304 steel and nickel alloy 718 and showed that the FCGR of both materials was positively correlated with B. Sriharsha et al. [22] performed FCG tests on compact tension (CT)

specimens of A533B pressure vessel steel with thicknesses of 10 mm and 20 mm. Their findings indicated that specimen size had minimal influence on crack growth behavior under the tested conditions, highlighting that the effect of thickness on FCG characteristics is highly material-specific.

In summary, the current research on FCG behavior of marine steel mainly focuses on the effects of single factors such as low temperature, R, R_{ol}, weld residual stress, and microstructure. Despite the critical importance of structural design for polar equipment operating in complex environments, existing studies and fundamental data concerning how load types and specimen dimensions affect the FCG behavior of marine steels at low temperatures remain insufficient. On the base of this, this study comprehensively explores the FCG behavior of DH36 steel under the combined effect of low temperature, R, R_{ol}, and B, so as to provide a theoretical basis and data support for the fatigue-resistant design of polar ship structures and green navigation.

2. Test Details

2.1. Test Material

DH36 steel, as a high-strength, high-toughness, low-alloy marine steel, was commonly used in polar ship equipment structures, such as open decks of polar ships, side bulkheads above the cold water line (CWL), and transverse bulkheads, etc. [23–25]. The elemental composition of DH36 steel is summarized in Table 1. (by ZSX Primus IV), which meets the certification standards of the ABS and CCS. The microstructure of the DH36 steel mainly consists of ferrite (F) and pearlite (P), as shown in Figure 1 (by VHX-7000).

Table 1. Main element content of DH36 steel.

DH36 Steel	C	Si	Mn	P	S	Cr
Test value	0.075	0.165	1.147	0.006	0.001	0.024
CCS standard	≤0.18	0.10–0.50	0.90–1.60	≤0.025	≤0.025	≤0.20
ABS standard	≤0.18	0.10–0.50	0.90–1.60	≤0.035	≤0.035	≤0.20

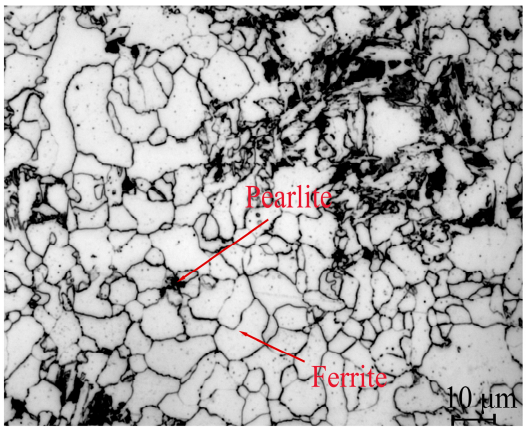


Figure 1. Microstructure of DH36 steel.

According to the investigation, the temperature range of the Arctic region was −60 °C to 20 °C [26,27], for which three temperature points were selected for the tests in this paper, which were 20 °C, −20 °C, and −60 °C, respectively. An MTS 810 fatigue testing machine with a 100 kN load capacity was used to perform the tensile and the fatigue crack growth FCG tests, as shown in Figure 2.

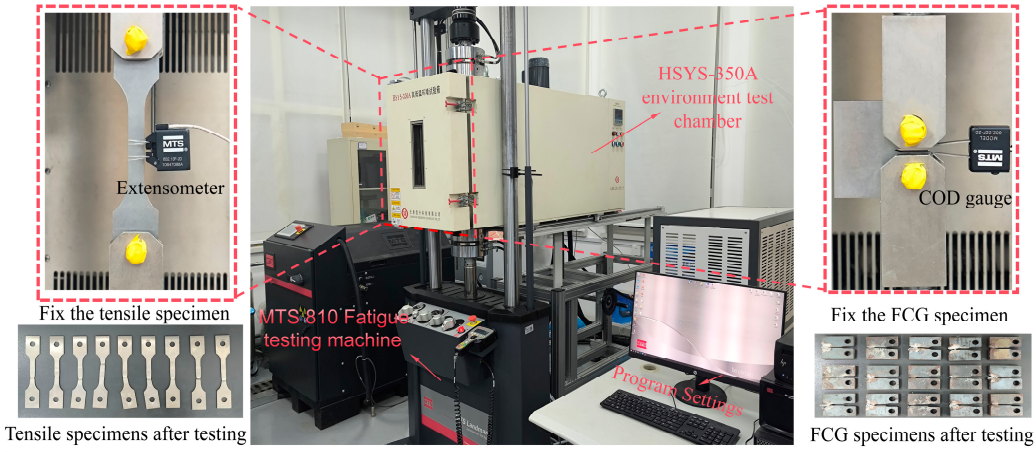


Figure 2. Test equipment.

2.2. Tensile Test

The tensile specimens were machined via wire cutting, followed by milling and grinding. To maintain data consistency, the loading direction was aligned with the rolling direction of the steel plates [28]. Figure 3 presents the specimen geometry, with a thickness of 3 mm. The test method was carried out with reference to the ASTM E8/M8-22 [29] specification. To ensure the uniformity of the specimen temperature, the test was started after the temperature was reduced to a preset value and held for 30 min. Each temperature point was tested three times to ensure result reliability.

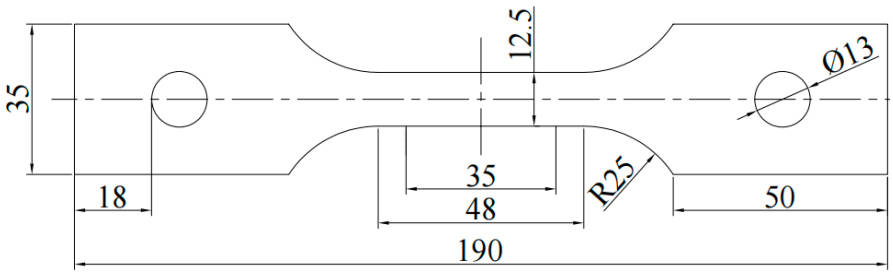


Figure 3. Dimension details of tensile specimens (mm).

2.3. FCG Test

2.3.1. Test Parameters

The FCG test method in this study was based on the ASTM E647-15 [30] specification using standard compact tensile (CT) specimens with dimensional details shown in Figure 4. The sampling process of the specimens ensured that the direction of crack growth was parallel to the rolling direction of the steel plate, thus ensuring the consistency of the test data [31]. The cracks of the CT specimens were prefabricated using the *K*-drop method [32] with a prefabricated crack length of 2 mm. After the prefabrication was completed, the CT specimen was placed in a low temperature room for cooling. After the temperature reached the set value, it was kept for 30 min before the experiment began. The tests were repeated at least three times under each test condition to ensure the reliability of the results.

According to the range of temperature changes in the Arctic, three temperature points (20 °C, −20 °C, and −60 °C) were selected for FCG tests. Based on the structural design requirements of polar ships, steel plates of 5 mm, 11.5 mm, and 18 mm thickness are widely used in different components. Thin plates (5 mm) are generally adopted in internal partition structures and non-load-bearing panels, whereas medium-thickness plates (11.5 mm) are commonly used in decks and shell plating exposed to polar conditions. Thick plates (18 mm) are essential in ice belt zones and keel structures where resistance to severe ice loads and

low temperature fracture is critical. Therefore, the thickness of CT specimens in this paper was selected as 5 mm, 11.5 mm, and 18 mm. For stress ratio and overload ratio, this paper refers to DNVGL-RP-C203 [33] and China Polar Ship Guide 2023 [34] as well as relevant literature [35–38] and adopts three R levels (0.1, 0.2, and 0.3) and two R_{ol} levels (1.5 and 2), respectively. The specific test parameters are shown in Tables 2–4, respectively, and the load spectra under constant amplitude and overload conditions is shown in Figure 5.

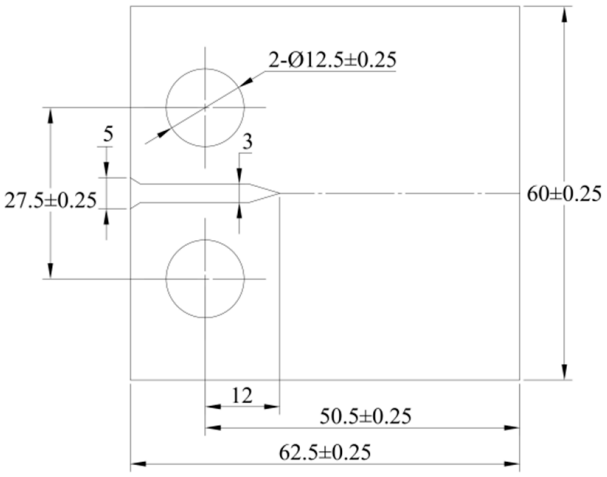


Figure 4. Details of FCG specimen size (mm).

Table 2. FCG test parameters for the combined action of temperature and R.

Number of Test Groups	Temperature (°C)	R	R_{ol}	B (mm)	F_{max} (kN)	F_{min} (kN)	f (Hz)
1	20/−20/−60	0.1	1.0	11.5	12.5	1.25	20
2		0.2				2.0	
3		0.3				3.75	

Table 3. FCG test parameters for the combination of temperature and R_{ol}.

Number of Test Groups	Temperature (°C)	R	R_{ol}	B (mm)	F_{max} (kN)	F_{min} (kN)	f (Hz)
1	20/−20/−60	0.1	1.0	11.5	12.5	1.25	20
2			1.5				
3			2.0				

Table 4. FCG test parameters for the combination of temperature and B.

Number of Test Groups	Temperature (°C)	R	R_{ol}	B (mm)	F_{max} (kN)	F_{min} (kN)	f (Hz)
1	20/−20/−60	0.1	1.0	5.0	12.5	1.25	20
2		0.2		11.5			
3		0.3		18.0			

2.3.2. Data Processing Methods

Paris law was commonly used to characterize the FCG behavior of marine materials. Here, C and m were constants fitted by

$$da/dN = C \cdot (\Delta K)^m \quad (1)$$

where C and m were material constants; ΔK was the stress intensity factor range, MPa·m$^{1/2}$.

In this study, the flexibility method [39] was used to record the crack size in real time, and the tension displacement value at the crack opening was measured in real time by

Crack Opening Displacement (COD) gauge, and the flexibility value corresponding to the current crack length was calculated by

$$U_0 = \left[\left(\frac{BEV_0}{F}\right)^{1/2} + 1\right]^{-1} \quad (2)$$

where U_0 is the flexibility value; B is the thickness of the specimen, mm; E denotes the modulus of elasticity, MPa; V_0 represents the tensile displacement at the crack opening, mm, and F is the applied load, N. Based on the flexibility value, the current crack size can be expressed by

$$a/W = 1.001 - 4.6695U_0 + 18.46{U_0}^2 - 236.82{U_0}^3 + 1214.9{U_0}^4 - 2143.6{U_0}^5 \quad (3)$$

where a is the crack length, mm; W is the width of the specimen, mm. According to GB/T 6398–2000 [40], the stress intensity factor range ΔK can be calculated by

$$\Delta K = \frac{\Delta P}{B\sqrt{W}} \frac{(2+\alpha)\left(0.886 + 4.64\alpha - 13.32\alpha + 14.75\alpha^3 - 5.6\alpha^4\right)}{(1-\alpha)^{3/2}} \quad (4)$$

Based on the experimental data of crack length and number of cycles obtained from the tests, a seven-point incremental polynomial [41] was fitted to them to obtain the fatigue crack growth rate (FCGR), which was solved as follows:

$$a_i = b_0 + b_1\left(\frac{2N_i - N_{i+3} - N_{i-3}}{N_{i+3} + N_{i-3}}\right) + b_2\left(\frac{2N_i - N_{i+3} - N_{i-3}}{N_{i+3} + N_{i-3}}\right)^2 \quad (5)$$

$$(da/dN_i) = \frac{2b_1(N_{i+3} - N_{i-3}) + 4b_2(2N_i - N_{i+3} - N_{i-3})}{(N_{i+3} + N_{i-3})^2} \quad (6)$$

where da/dN is the FCGR, mm/cycle; N_i is the number of cycles at any point i on the a-N curve; a_i is the crack length at the number of cycles N_i, mm; and b_0, b_1, and b_2 are the regression coefficients obtained by least squares fitting.

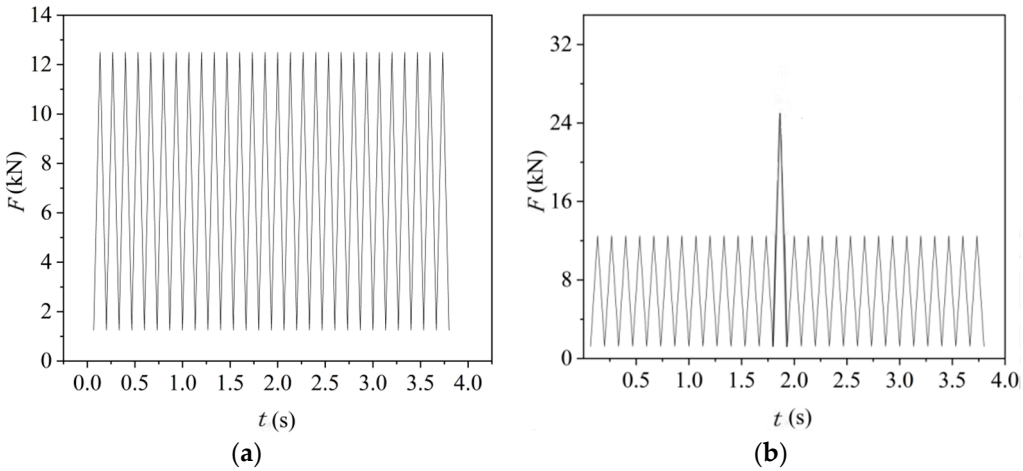


Figure 5. Load spectrum under constant amplitude and overload conditions: (**a**) constant amplitude; (**b**) overload.

3. Test Results and Discussion

3.1. Mechanical Properties of DH36 Steel at Different Temperatures

The stress-strain curves of DH36 steel at different temperatures were shown in Figure 6a. As the temperature decreases, the stress-strain curve of DH36 steel shows

an overall upward trend, and there is still an obvious yielding stage at −60 °C. According to Figure 6b and the data in Table 5, it can be seen that the yield strength f_s, tensile strength f_b, and modulus of elasticity E of DH36 steel increased by 5.07%, 9.06%, and 2.86%, respectively, with the decrease of the temperature from 20 °C to −20 °C. When the temperature was further reduced to −60 °C, the f_s, f_b, and E of DH36 steel increased by 5.81%, 4.56%, and 7.85%, respectively. On the whole, the f_s, f_b, and E of DH36 steel increased by 10.94%, 11.17%, and 14.04%, respectively, when the temperature was decreased from 20 °C to −60 °C. The above results indicate that the temperature has a significant effect on the mechanical properties of DH36 steel, and the low temperature enhanced the mechanical properties (f_s, f_b, and E) of DH36 steel.

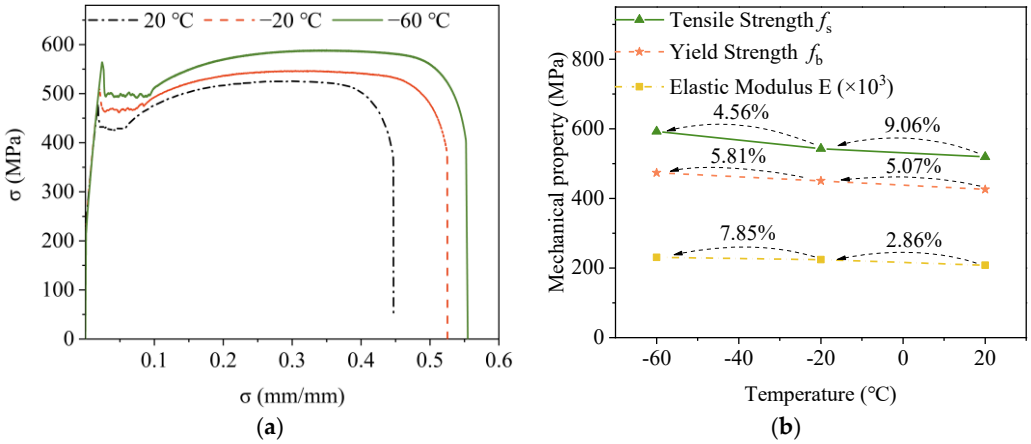


Figure 6. Comparison of the mechanical properties at different temperatures: (**a**) stress-strain curve; (**b**) mechanical properties of DH36 steels.

Table 5. Mechanical property parameters of DH36 steel.

Temperature (°C)	E (GPa)	f_s (MPa)	f_b (MPa)
20	207.81	426.05	519.41
−20	224.13	450.80	543.10
−60	230.55	473.64	592.33

3.2. FCG Behavior of DH36 Steel Under the Combined Effect of Temperature and R_{ol}

As seen in Figure 7, after the occurrence of overload, the FCGR of DH36 steel shows a process of rapid decrease, slow recovery, and final restoration of the original rate [42], and the rate change area shows a typical "triangular feature". In order to quantitatively analyze the effect of overload on FCGR, this study defines the FCGR at the lowest point after overload as V_L, the FCGR before overload as V_a, and the area surrounded by the "triangular feature" as S_a.

Table 6 demonstrates the comparison results of each characteristic parameter. The results showed that when the R_{ol} was 1.5, as the temperature decreased from 20 °C to −20 °C, V_a and V_L decreased by 5.22% and 2.36%, respectively; and when the temperature was further decreased to −60 °C, V_a and V_L again decreased by about 11.38% and 8.14%, respectively. When the R_{ol} was 2, as the temperature decreased from 20 °C to −20 °C, V_a and V_L decreased by 13.30% and 14.16%, respectively; and when the temperature was further decreased to −60 °C, V_a and V_L again decreased by about 32.89% and 21.13%. The above results indicate that the temperature has a significant effect on the FCG behavior of DH36 steel, and the FCGR decreases significantly with decreasing temperature. However, when R_{ol} was 1.5 and 2, S_a decreased by 22.90% and 42.67%, respectively, as the temperature decreased from 20 °C to −20 °C; further decreasing to −60 °C, S_a decreased by 73.57%

and 63.88%, respectively. The above results show that the crack growth retardation effect induced by overload in DH36 steel was significantly diminished with decreasing temperature, and the extent of this reduction becomes more pronounced at lower temperatures.

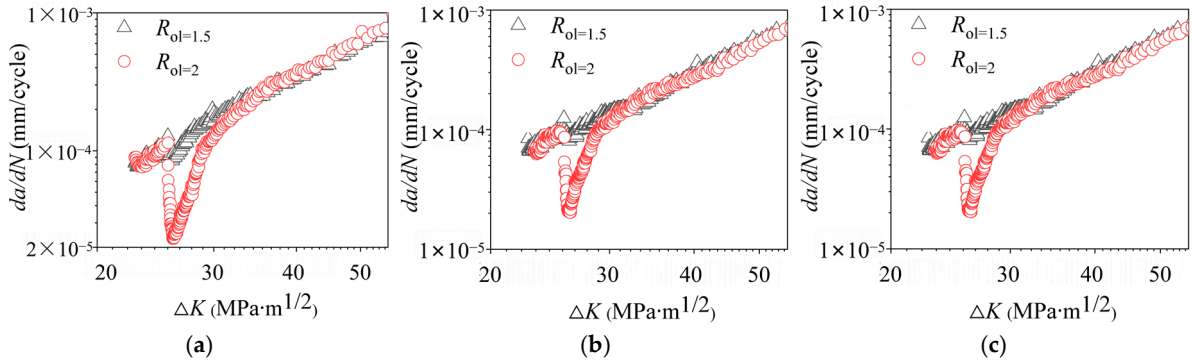


Figure 7. da/dN-ΔK relationship curves at different R_{ol} and temperatures: (**a**) 20 °C; (**b**) −20 °C; (**c**) −60 °C.

Table 6. Characteristic coefficients describing the overload effect.

Temperature (°C)	R_{ol}	V_a	V_L	S_a	FCG Life (N)
20	1.5	1.15×10^{-4}	8.05×10^{-5}	3.10×10^{-5}	73,352
	2.0	1.15×10^{-4}	2.26×10^{-5}	2.25×10^{-5}	114,216
−20	1.5	1.09×10^{-4}	7.86×10^{-5}	2.39×10^{-5}	87,240
	2.0	9.97×10^{-5}	1.94×10^{-5}	1.29×10^{-4}	117,876
−60	1.5	9.66×10^{-5}	7.22×10^{-5}	6.32×10^{-6}	122,324
	2.0	6.69×10^{-5}	1.53×10^{-5}	4.66×10^{-5}	142,942

From Figure 8, it can be seen that the a-N curve of DH36 steel first tends to be horizontal during the overload process and then gradually returns to its initial state. At the same temperature, the FCG life is significantly extended with the increase of R_{ol}. Table 6 and Figure 9 show that under the three temperature conditions of 20 °C, −20 °C, and −60 °C, when R_{ol} increases from 1.5 to 2, the FCG life of DH36 steel increases by 55.71%, 35.12%, and 16.86%, respectively. This suggests that, although the increase of R_{ol} significantly extended the FCG life, low temperature significantly weakens the overload retardation effect.

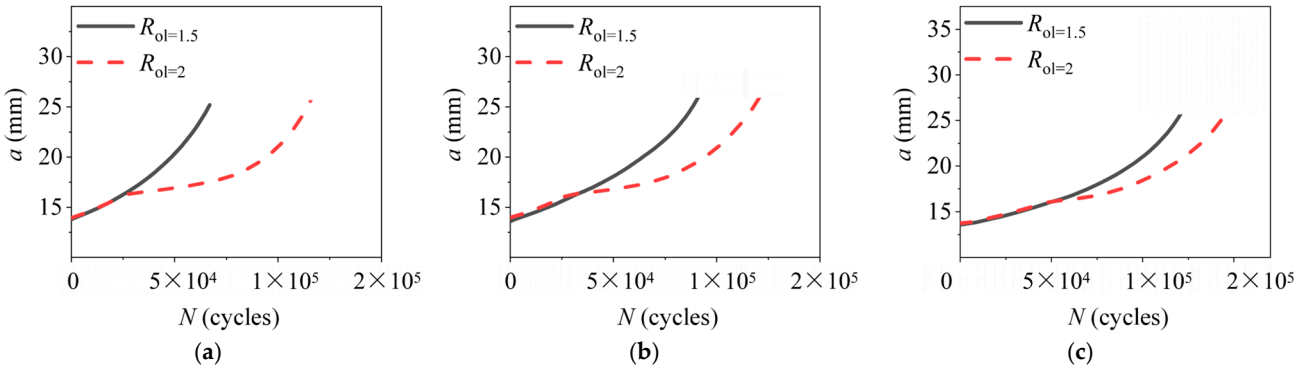


Figure 8. a-N curves at different R_{ol} and temperatures: (**a**) 20 °C; (**b**) −20 °C; (**c**) −60 °C.

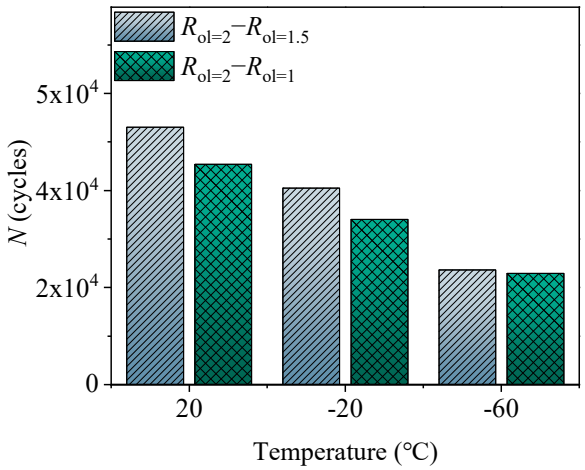


Figure 9. Comparison of FCG increment of DH36 steel under low temperature overload.

The above experimental results show that the FCG behavior of DH36 steel under overload presents a typical "triangular characteristic", and the temperature has a significant effect on the FCG behavior: as the temperature decreases, the retardation effect becomes less pronounced. Additionally, under the same temperature conditions, higher R_{ol} leads to longer FCG life, however, the effectiveness of R_{ol} is markedly diminished at lower temperatures.

3.3. FCG Behavior of DH36 Steel Under the Combined Effect of Temperature and R

The FCGR-ΔK relationship curves for DH36 steel at different R and temperatures were shown in Figure 10. The results show that, with the peak load F_{max} remaining constant, both the initial stress intensity factor range ΔK_0 and the termination stress intensity factor range ΔK_e decrease significantly with increasing R. Specifically, at 20 °C, −20 °C, and −60 °C, when R increased from 0.1 to 0.3, the changes of ΔK_0 were in the range of 23.60 MPa·m$^{1/2}$ to 17.84 MPa·m$^{1/2}$, 22.59 MPa·m$^{1/2}$ to 17.51 MPa·m$^{1/2}$, and 21.88 MPa·m$^{1/2}$ to 17.54 MPa·m$^{1/2}$, respectively, and the changes of ΔK_e were in the range of 61.84 MPa·m$^{1/2}$ to 45.17 MPa·m$^{1/2}$, 60.10 MPa·m$^{1/2}$ to 45.71 MPa·m$^{1/2}$, and 61.13 MPa·m$^{1/2}$ to 47.06 MPa·m$^{1/2}$. It can be seen that the increase of R value significantly reduces the range of effective driving force during crack growth. However, the FCGR-ΔK relationship curves at different R (0.1, 0.2, and 0.3) are not significantly different in the stable crack growth stage, and the curves are concentrated in a narrow scatter interval.

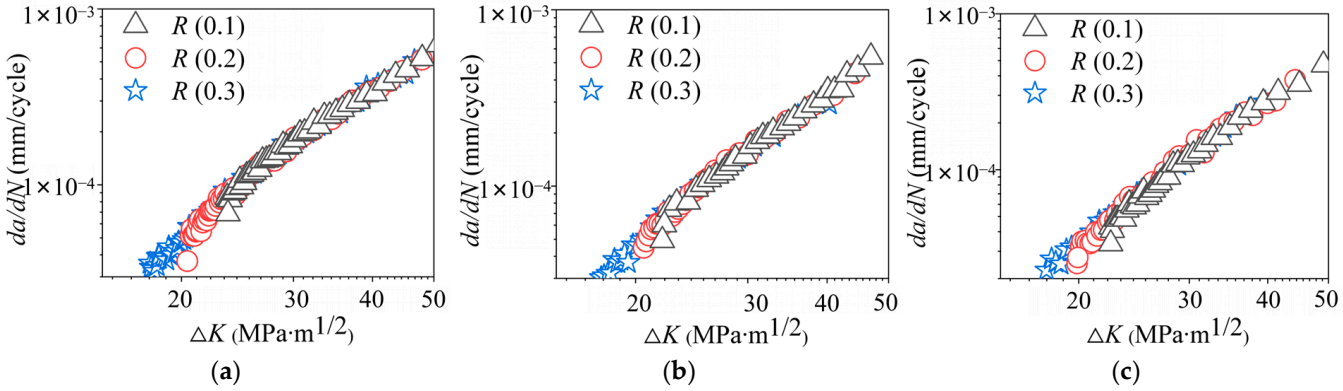


Figure 10. Curves of the da/dN-ΔK relationship at different R: (**a**) 20 °C; (**b**) −20 °C; (**c**) −60 °C.

Figure 11 further demonstrates the FCGR-ΔK relationship for the three thickness specimens under different temperature conditions, and The Paris parameters (lgC and m) of

DH36 steel for each R and temperature combination are shown in Table 7. The results show that the FCGR of DH36 steel decreases with decreasing temperature under different R.

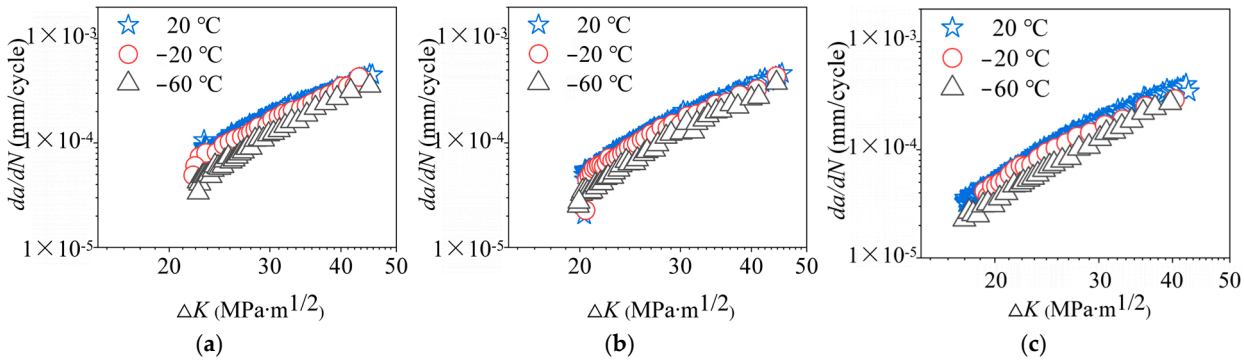


Figure 11. Curves of the da/dN-ΔK relationship at different temperatures: (**a**) 0.1; (**b**) 0.2; (**c**) 0.3.

Table 7. Paris parameters of DH36 steel at different temperatures and R.

Test Temperature (°C)	R	R_{ol}	B (mm)	lg$C$	m	FCG Life (N)
20	0.1	1.0	11.5	−7.679	2.761	66,448
−20				−7.710	2.720	81,423
−60				−8.830	3.401	121,678
20	0.2		11.5	−8.780	2.821	102,336
−20				−7.761	2.748	115,485
−60				−8.145	2.908	155,214
20	0.3		11.5	−8.723	3.770	151,265
−20				−8.910	3.629	169,011
−60				−9.144	3.714	250,981

Comparison of the FCG life at different R (Figure 12 and Table 7) showed that at 20 °C, the FCG life increased by 54.01% when R was increased from 0.1 to 0.2, and by 47.81% when it was increased from 0.2 to 0.3; at −20 °C, it increased by 41.83% and 46.34%, respectively; and at −60 °C, it increased by 21.56% and 67.69%. This indicates that the FCG life of DH36 steel is significantly prolonged with increasing R under constant F_{max} conditions, and as shown in Figure 13, this prolongation effect was further strengthened by the low temperature environment.

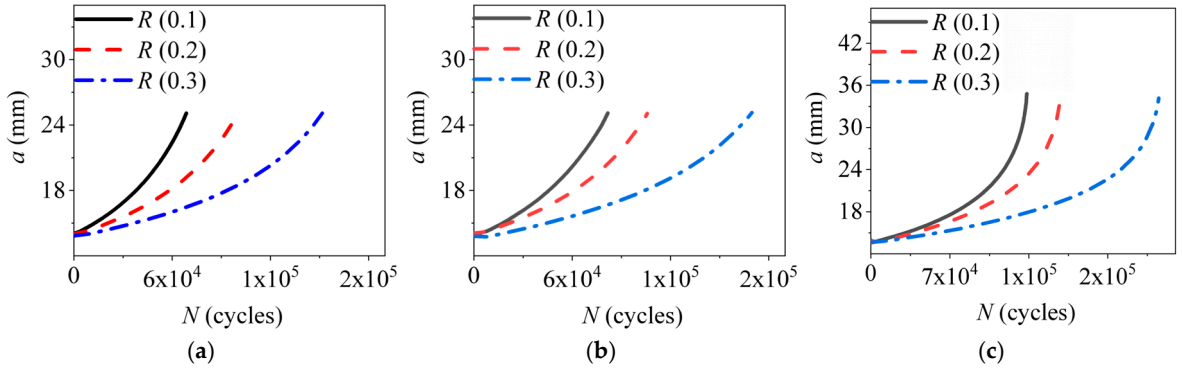


Figure 12. a-N relation curves at different R and temperatures: (**a**) 20 °C; (**b**) −20 °C; (**c**) −60 °C.

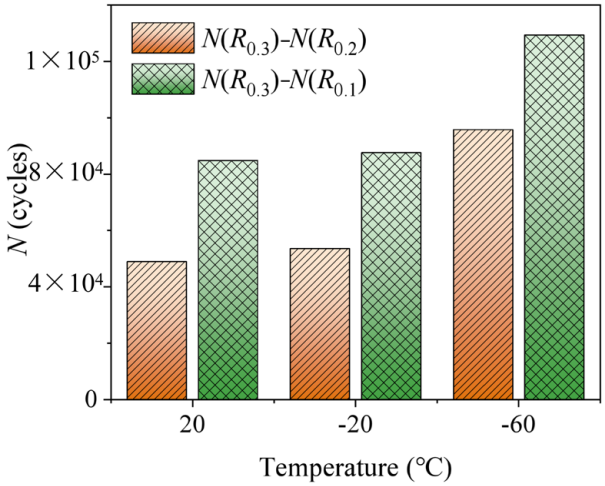


Figure 13. Comparison of FCG increment of DH36 steel at different temperatures and *R*.

3.4. FCG Behavior of DH36 Steel Under the Combined Effect of Temperature and B

It has been shown that there is a certain coupling effect between the plate thickness and the ambient temperature on the mechanical properties of the material [41–44]. It was found that the impact performance of the reinforced plate structure was significantly better than that of the unreinforced plate at room temperature environments, but it shows the opposite trend in low temperature environments, indicating that there was a complex interaction between the *B* of the marine steel and the temperature. In order to deeply investigate the combined effect of *B* and temperature of DH36 steel on the FCG behavior of marine steel, this study carries out systematic FCG tests at three temperatures, 20 °C, −20 °C, and −60 °C, for three common plate thicknesses (5 mm, 11.5 mm, and 18 mm) of DH36 steel used in ship structures.

The FCGR-Δ*K* curves of DH36 steel at different *B*, shown in Figure 14a–c, indicate that the FCGR of DH36 steel increases with increasing *B*. Moreover, in the range of higher Δ*K*, the curves of specimens with various *B* tend to converge and eventually concentrate in a narrower scatter band. This convergence phenomenon indicates that the effect of *B* on FCGR diminishes with increasing Δ*K*.

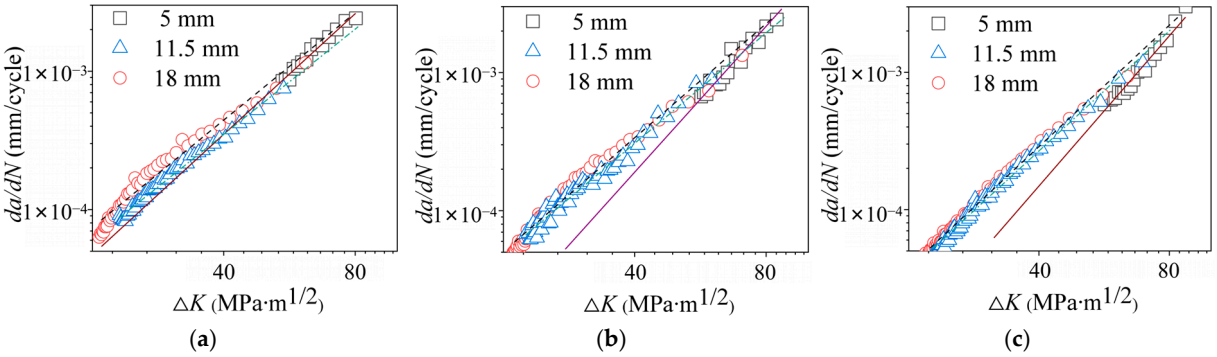


Figure 14. *da*/*dN*-Δ*K* relationship curves at different *B* and temperatures: (**a**) 20 °C; (**b**) −20 °C; (**c**) −60 °C.

Figure 15 further demonstrates the FCGR-Δ*K* relationship for the three thickness specimens under different temperature conditions, and the Paris parameters under different conditions are shown in Table 8.

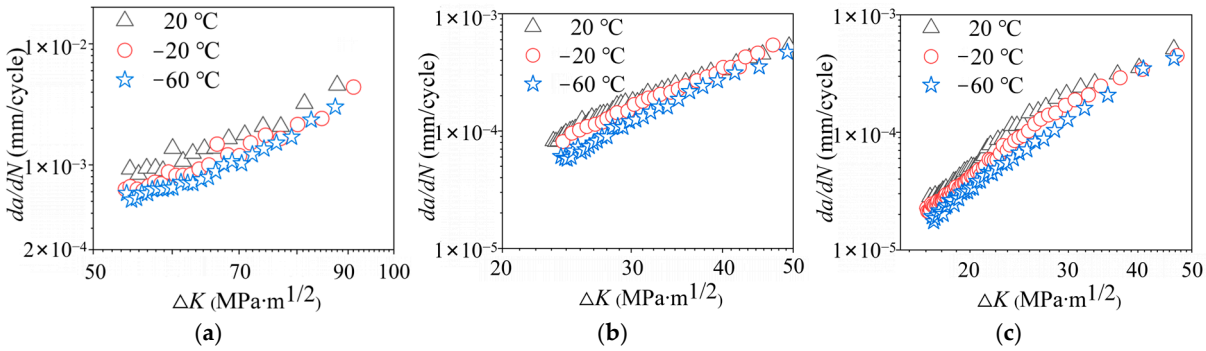


Figure 15. Comparison of FCGR-Δ*K* relationship curves of three thickness samples under different temperature conditions: (**a**) 5 mm; (**b**) 11.5 mm; (**c**) 18 mm.

Table 8. Crack growth parameters at different *B* and temperatures.

Test Temperature (°C)	*R*	*B*	lg*C*	*m*	FCG Life (N)
20	0.1	5.0	−7.087	2.955	8140
−20			−7.057	3.210	10,485
−60			−7.069	3.085	12,285
20	0.1	11.5	−7.679	2.761	66,448
−20			−7.710	2.720	81,423
−60			−8.830	3.401	121,678
20	0.1	18	−8.396	3.195	279,892
−20			−8.050	3.724	315,738
−60			−9.744	3.284	482,169

From Figure 16, it can be seen that there are obvious differences in the *a*-*N* curves of DH36 steel at different *B*. Under the same loading condition, the thinner the sample is, the lower the FCG life is. Although the thicker samples showed higher FCGR, since F_{max} and *R* remained constant during loading, and the initial Δ*K* value was not equal in this study, the increase of *B* also resulted in the decrease of ΔK_0. At 20 °C, the ΔK_0 was 14.97 MPa·m$^{1/2}$, 23.45 MPa·m$^{1/2}$, and 54.12 MPa·m$^{1/2}$ for the thickness specimens with 18 mm, 11.5 mm, and 5 mm, respectively. Due to the significant difference in the crack growth driving force, the thin plate specimens, despite the lower FCGR, endured a higher Δ*K* throughout the loading history, resulting in a significantly shorter FCG life. As shown in Figure 17, the FCG life decreased by 76.25% when the *B* was decreased from 18 mm to 11.5 mm at 20 °C and by 87.75% when decreased from 11.5 mm to 5 mm. This trend was still significant at −20 °C versus −60 °C ($\Delta N_{11.5\text{-}5}$ was 87.12% and 89.90%, and $\Delta N_{18\text{-}11.5}$ was 74.21% and 74.76%, respectively). The results show that the variation of temperature affects the FCG life of different *B* to a generally consistent extent under the same loading conditions.

In summary, the results indicate that thickness and temperature independently exert significant effects on the FCG behavior of DH36 steel, with no evident interaction observed under the current experimental conditions. However, the reduction in specimen thickness substantially decreases FCG life, suggesting that the variations in *B* should be carefully considered in the lightweight design of polar marine steel structures to ensure adequate fatigue durability.

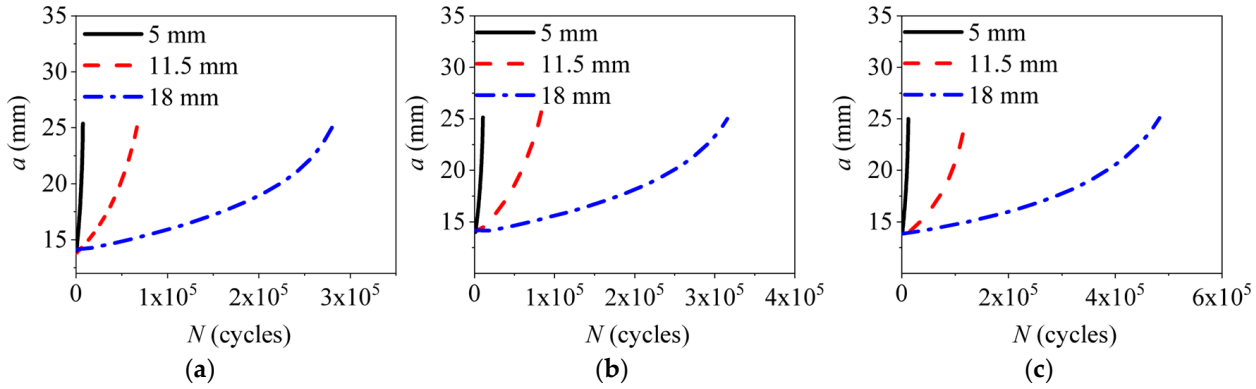


Figure 16. *a*-*N* relationship curves at different *B* and temperatures: (**a**) 20 °C; (**b**) −20 °C; (**c**) −60 °C.

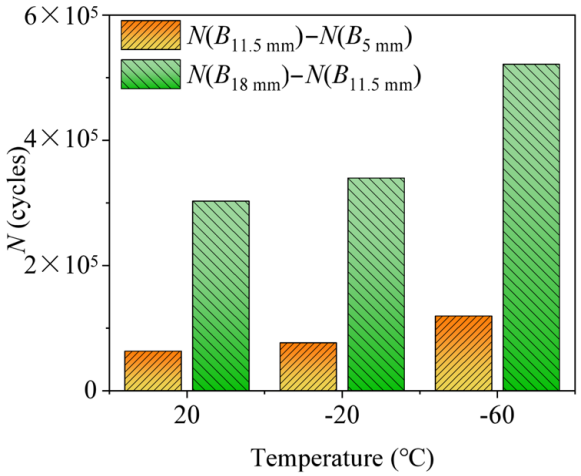


Figure 17. Comparison of the increment of FCG caused by *B* at different temperatures.

3.5. Comparison of FCG Rate of DH36 Steel and Other Marine Steels at Low Temperature

Due to the limited number of studies focusing on the FCG behavior of marine steels under combined low temperature and loading conditions, this paper compares the FCGR of three representative marine steels (DH36, EH36, and EQ70) under identical testing conditions. The comparative results are shown in Figure 18, with reference data provided in [45].

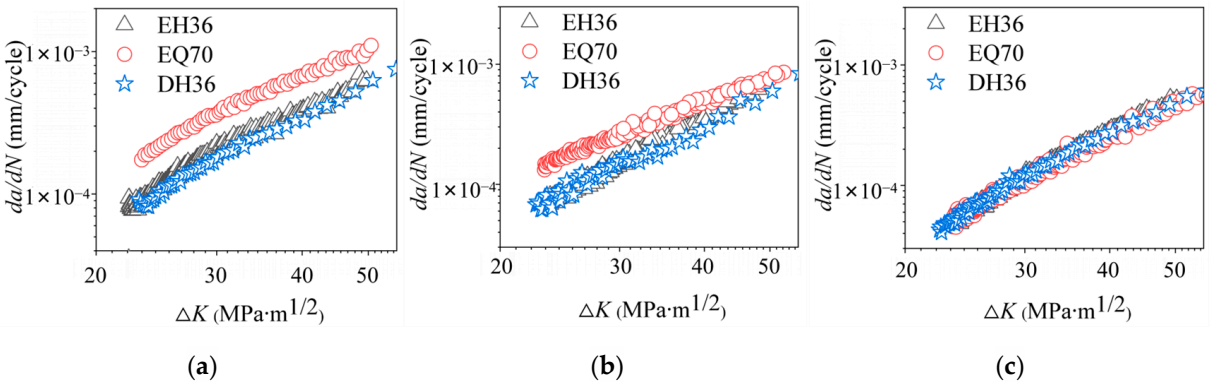


Figure 18. Comparison of da/dN-ΔK relationship curves of three kinds of marine steel at different temperatures: (**a**) 20 °C; (**b**) −20 °C; (**c**) −60 °C.

The results indicate that at 20 °C, the FCGR of DH36 steel is slightly lower than that of EH36 and significantly lower than that of EQ70, suggesting that DH36 exhibits superior resistance to FCG at room temperature. When the temperature decreases to −20 °C, the

difference in FCGR between DH36 and EH36 becomes smaller, and both materials still outperform EQ70. Further reduction in temperature to −60 °C leads to a convergence of the FCGR-ΔK data for all three steels within a narrow scatter band, indicating that the differences in fatigue crack growth rates among DH36, EH36, and EQ70 become significantly reduced at extremely low temperatures.

To more clearly compare the influence of temperature on the FCGR of the three marine steels, three ΔK levels (25 MPa·m$^{1/2}$, 35 MPa·m$^{1/2}$, and 45 MPa·m$^{1/2}$) were selected for comparative analysis across different temperatures, as shown in Figure 19. As the temperature decreased from 20 °C to −20 °C, the FCGR of all three steels decreased to varying degrees at each ΔK level, with EQ70 exhibiting a slightly larger reduction than DH36 and EH36. When the temperature was further reduced from −20 °C to −60 °C, the FCGR of EH36 and EQ70 showed a greater reduction compared to the previous stage (20 °C to −20 °C). However, DH36 showed a similar trend only when ΔK was 25 MPa·m$^{1/2}$; with increasing ΔK, the reduction in FCGR for DH36 became less pronounced. This behavior suggests that DH36 may have undergone a fatigue ductile-to-brittle transition in the temperature range of −20 °C to −60 °C, consistent with the findings reported in [14].

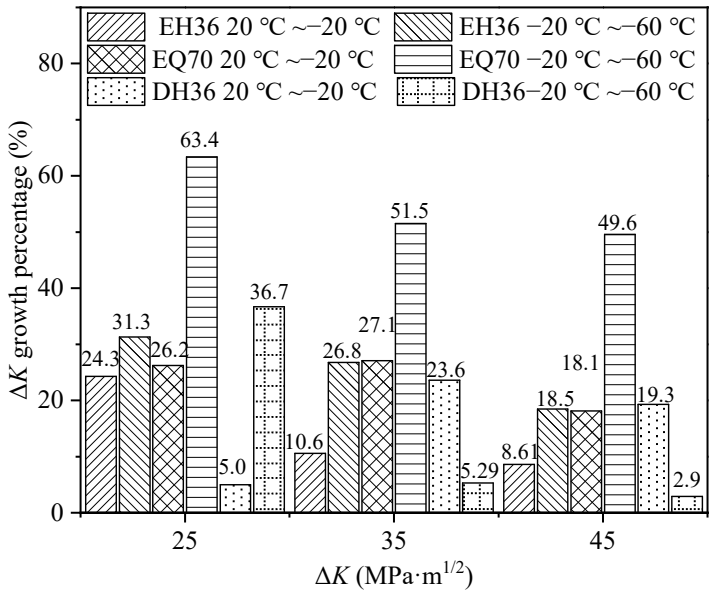


Figure 19. Comparison of percentage change of three marine steels' FCGR at different temperatures.

The comparison of Paris law parameters (C and m) for DH36, EH36, and EQ70 steels at low temperatures is presented in Table 9 [45]. As the temperature decreases, the log$C$ values of all three steels show a decreasing trend, while the m values generally increase. DH36 and EH36 exhibit similar log$C$ values, both of which are lower than that of EQ70. Similarly, the m values of DH36 and EH36 are close to each other and higher than that of EQ70.

Table 9. Comparison of c and m values of EH36, EQ70, and D36 steels at different temperatures.

Material	Test Temperature (°C)	lg$C$	m	R	B (mm)
EH36	20/−20/−60	−7.564/−8.299/−8.681	2.601/3.032/3.202	0.1	11.5
EQ70	20/−20/−60	−6.772/−6.939/−8.340	2.251/2.292/2.960	0.1	11.5
DH36	20/−20/−60	−7.679/−7.771/−8.830	2.761/2.72/3.401	0.1	11.5

4. Conclusions

The fatigue life of each component is made up of two separate phases: nucleation and growth; to properly choose a material that has the best performance in terms of fatigue life, it is necessary to evaluate both of these phases. This paper reveals the FCG behavior of polar marine steel under the combined effects of low temperature and overload ratio R_{ol}, low temperature and specimen thickness B, and low temperature and stress ratio R. The main conclusions of this study are as follows:

(1) The mechanical properties of DH36 steel were enhanced by decreasing temperature in the Arctic temperature range. The yield strength, tensile strength, and modulus of elasticity of DH36 steel increased by 10.94%, 11.17%, and 14.04%, respectively, when the temperature was decreased from 20 °C to −60 °C.

(2) In the range of −60 °C to −20 °C, the combined effect of low temperature overload leads to an overall significant decrease in the FCGR of DH36 steel, and the FCG life of DH36 steel is positively correlated with R_{ol}. However, this retardation effect is significantly weakened as the temperature decreases, and the lower the temperature, the more obvious the weakening of the retardation effect; thus, increasing the risk of structural fatigue failure. Therefore, the degradation of the retardation effect of crack expansion under low temperature should be fully considered in the design and operation of ship structures to ensure service safety and structural reliability.

(3) Under the condition that the peak load F_{max} is kept constant, as the stress ratio R rises from 0.1 to 0.3, the initial stress intensity factor ΔK_0 and the terminal stress intensity factor ΔK_e of the DH36 steel at the same crack length are both significantly reduced; meanwhile, the FCG life is significantly extended with the elevation of R. In addition, the low temperature environment further reinforces the effect of elevated R on extending FCG life.

(4) In the range of −60 °C to −20 °C, the FCGR of DH36 steel increases with increasing plate thickness, but the rate of increase decreases as ΔK increases. Lowering the temperature and increasing the specimen thickness significantly shortens the FCG life in thinner specimens due to higher initial stress intensity factors. This conclusion indicates that the impact of thickness on fatigue performance in polar ship steel structures cannot be overlooked in lightweight design and anti-fatigue optimization.

This paper provides key data for lightweight design and anti-fatigue optimization of polar engineering and ships and lays a theoretical foundation for the safety assessment and life prediction of polar marine steel structures. Future work will further focus on the effects of low temperature corrosion and complex loading conditions on the fatigue performance of polar marine steel structures in order to realize more comprehensive safety assessment and prediction.

Author Contributions: Investigation, writing—original draft preparation, K.Q.; conceptualization, funding acquisition, writing—review and editing, supervision, Z.L.; methodology, X.W.; software, Z.S.; validation, Q.G. All authors have read and agreed to the published version of the manuscript.

Funding: This work is supported by the National Natural Science Foundation of China (Grant Nos. 52371361 and 51879026), the Dalian Science and Technology Innovation Fund Project (Grant No. 2020JJ25CY016), and the Fundamental Research Funds for the Central Universities of China (Grant Nos. 3132023516 and 3132023606).

Institutional Review Board Statement: Not applicable.

Informed Consent Statement: Not applicable.

Data Availability Statement: The original contributions presented in this study are included in the article. Further inquiries can be directed to the corresponding author.

Acknowledgments: This research is supported by Dalian Shidao Industry Co., Ltd.

Conflicts of Interest: The authors declare no conflicts of interest.

References

1. Yang, X.; Lin, Z.Y.; Zhang, W.J.; Xu, S.; Zhang, M.Y.; Wu, Z.D.; Han, B. Review of risk assessment for navigational safety and supported decisions in arctic waters. *Ocean Coast. Manag.* **2024**, *247*, 106931. [CrossRef]
2. Adumene, S.; Ikue-John, H. Offshore system safety and operational challenges in harsh Arctic operations. *J. Saf. Sci. Resil.* **2022**, *3*, 153–168. [CrossRef]
3. Yan, X.; Huang, X.; Huang, Y.; Cui, W. Prediction of fatigue crack growth in a ship detail under wave-induced loading. *Ocean Eng.* **2016**, *113*, 246–254. [CrossRef]
4. Braun, M.; Ehlers, S. Review of methods for the high-cycle fatigue strength assessment of steel structures subjected to sub-zero temperature. *Mar. Struct.* **2022**, *82*, 103153. [CrossRef]
5. Xiao, Q.; Xie, Y.; Hu, F.; Hu, C. Current Status and Trends of Low-Temperature Steel Used in Polar Regions. *Materials* **2024**, *17*, 3117. [CrossRef]
6. Dong, Y.; Garbatov, Y.; Soares, C.G. Review on uncertainties in fatigue loads and fatigue life of ships and offshore structures. *Ocean Eng.* **2022**, *264*, 112514. [CrossRef]
7. Wang, Y.; Liu, J.; Hu, J.; Garbatov, Y.; Soares, C.G. Fatigue strength of EH36 steel welded joints and base material at low-temperature. *Int. J. Fatigue* **2021**, *142*, 105896. [CrossRef]
8. Vecchiato, L.; Campagnolo, A.; Meneghetti, G. Numerical calibration and experimental validation of the direct current potential drop (DCPD) method for fracture mechanics fatigue testing of single-edge-crack round bars. *Int. J. Fatigue* **2021**, *150*, 106316. [CrossRef]
9. Warren, M.F.; Ali-Lavroff, J.; Holloway, D.; Magoga, T. Comparing linear damage hypothesis to linear elastic fracture mechanics in the estimation of fatigue life in a high speed light craft. *Ocean Eng.* **2023**, *290*, 116338. [CrossRef]
10. Kruke, B.I.; Auestad, A.C. Emergency preparedness and rescue in Arctic waters. *Saf. Sci.* **2021**, *136*, 105163. [CrossRef]
11. Igwemezie, V.; Mehmanparast, A.; Brennan, F. The influence of microstructure on the fatigue crack growth rate in marine steels in the Paris Region. *Fatigue Fract. Eng. Mater. Struct.* **2020**, *43*, 2416–2440. [CrossRef]
12. Shen, X.; Gao, X.; Shao, Y.; He, W.; Yu, Z. Investigation on the fatigue crack growth behavior of welded joints in EH690 high-strength marine steel. *Int. J. Fatigue* **2024**, *189*, 108572. [CrossRef]
13. Wang, C.; Wang, S.; Xie, L.; Liu, Y.; Deng, J.; He, W. Fatigue crack growth behavior of marine steel under variable amplitude loading-combining DIC technique and SEM observation. *Int. J. Fatigue* **2023**, *170*, 107508. [CrossRef]
14. Zhao, W.; Feng, G.; Ren, H.; Leira, B.J.; Zhang, M. Temperature-dependent characteristics of DH36 steel fatigue crack propagation. *Fatigue Fract. Eng. Mater. Struct.* **2020**, *43*, 617–627. [CrossRef]
15. Tu, W.; Yue, J.; Xie, H.; Tang, W. Fatigue crack propagation behavior of high-strength steel under variable amplitude loading. *Eng. Fract. Mech.* **2021**, *247*, 107642. [CrossRef]
16. Qin, D.; Xiayang, L.; Geng, X. Experimental study on low-cycle fatigue characteristics of marine structural steel. *J. Mar. Sci. Eng.* **2024**, *12*, 651. [CrossRef]
17. Li, Y.; Guo, W.; Cao, C.; Li, M.; Wu, Z.; Wang, T.; Pan, X. Experimental Study on the Fatigue Crack Propagation Rate of 925A Steel for a Ship Rudder System. *Materials* **2024**, *17*, 1808. [CrossRef]
18. Song, W.; Man, Z.; Xu, J.; Wang, X.; Liu, C.; Zhou, G.; Berto, F. Fatigue crack growth behavior of different zones in an overmatched welded joint made with D32 marine structural steel. *Metals* **2023**, *13*, 535. [CrossRef]
19. Wang, K.; Wu, L.; Li, Y.Z.; Qin, C. Experimental study on low temperature fatigue performance of polar icebreaking ship steel. *Ocean Eng.* **2020**, *216*, 107789. [CrossRef]
20. Buixadé Farré, A.; Stephenson, S.R.; Chen, L.; Czub, M.; Dai, Y.; Demchev, D.; Wighting, J. Commercial Arctic shipping through the Northeast Passage: Routes, resources, governance, technology, and infrastructure. *Polar. Gogr.* **2014**, *37*, 298–324. [CrossRef]
21. Park, H.B.; Lee, B.W. Effect of specimen thickness on fatigue crack growth rate. *Nucl. Eng. Des.* **2000**, *197*, 197–203. [CrossRef]
22. Sriharsha, H.K.; Pandey, R.K.; Chatterjee, S. Towards standardising a sub-size specimen for fatigue crack propagation behaviour of a nuclear pressure vessel steel. *Eng. Fract. Mech.* **1999**, *64*, 607–624. [CrossRef]
23. Zhao, W.; Feng, G.; Zhang, M.; Ren, H.; Sinsabvarodom, C. Effect of low temperature on fatigue crack propagation rates of DH36 steel and its butt weld. *Ocean Eng.* **2020**, *196*, 106803. [CrossRef]
24. Zhao, W.; Feng, G.; Liu, W.; Ren, H. Research on fatigue properties of typical welded joints of DH36 steel at −60 °C. *Appl. Sci.* **2020**, *10*, 3742. [CrossRef]
25. Clayton, D.K.; Saleh, M.; Ferguson, T.M.; Ojeda, R. Effects of fatigue damage on the high strain-rate performance of DH36 steel. *Ships Offshore Struct.* **2022**, *17*, 646–660. [CrossRef]

26. Zhang, T.; Chen, M.T.; Cai, A.; Cao, H.; Yun, X.; Zhao, H.; Zhang, Y. Behaviour of high strength steel butt joints exposed to arctic low temperatures. *Thin-Walled Struct.* **2023**, *192*, 111157. [CrossRef]
27. Guo, W.; Yu, L.; Wu, Z.; Zhang, Y.; Cao, C.; Zeng, Y.; Huang, J. Effect of low temperature on the fatigue crack propagation behavior of underwater manned vehicle rudder materials in Arctic environments. *ACS Omega* **2024**, *9*, 38925–38935. [CrossRef]
28. Motra, H.B.; Hildebrand, J.; Dimmig-Osburg, A. Influence of specimen dimensions and orientation on the tensile properties of structural steel. *Mater. Test.* **2014**, *56*, 929–936. [CrossRef]
29. *ASTM Standard E8/E8-22*; Standard Test Methods for Tension Testing of Metallic Materials. ASTM International: West Conshohocken, PA, USA, 2022. Available online: http://www.astm.org (accessed on 2 January 2025).
30. *ASTM Standard E647-15*; Standard Test Method for Measurement of Fatigue Crack Growth Rates. ASTM International: West Conshohocken, PA, USA, 2015. Available online: http://www.astm.org (accessed on 6 January 2025).
31. Niendorf, T.; Rubitschek, F.; Maier, H.J.; Canadinc, D.; Karaman, I. On the fatigue crack growth–microstructure relationship in ultrafine-grained interstitial-free steel. *J. Mater. Sci.* **2010**, *45*, 4813–4821. [CrossRef]
32. Wang, C.; Yang, B.; Zhu, T.; Zhou, S.; Xiao, S.; Yang, G. Effect of different regions on fatigue crack growth behavior of 6005-T6 aluminum alloy metal inert gas (MIG) butt welded joint: Experimental and numerical study. *Weld. World* **2024**, *68*, 2109–2123. [CrossRef]
33. DNV GL. *DNVGL-RP-C203: Fatigue Design of Offshore Steel Structures*; Det Norske Veritas Germanischer Lloyd: Høvik, Norway, 2016; Available online: https://www.dnv.com (accessed on 3 January 2025).
34. China Classification Society (CCS). *Guidelines for Polar Class Ships*; China Classification Society: Beijing, China, 2023; Available online: https://www.ccs.org.cn (accessed on 6 January 2025). (In Chinese)
35. Dai-Heng, C.; Hironobu, N. Analysis of the delaying effects of overloads on fatigue crack propagation. *Eng. Fract. Mech.* **1991**, *39*, 287–298. [CrossRef]
36. Bathias, C.; Vancon, M. Mechanisms of overload effect on fatigue crack propagation in aluminium alloys. *Eng. Fract. Mech.* **1978**, *10*, 409–424. [CrossRef]
37. Datta, S.; Chattopadhyay, A.; Iyyer, N.; Phan, N. Fatigue crack propagation under biaxial fatigue loading with single overloads. *Int. J. Fatigue* **2018**, *109*, 103–113. [CrossRef]
38. Ding, Z.; Wang, X.; Gao, Z.; Bao, S. An experimental investigation and prediction of fatigue crack growth under overload/underload in Q345R steel. *Int. J. Fatigue* **2017**, *98*, 155–166. [CrossRef]
39. Lee, B.S.; Kim, J.M.; Kwon, J.Y.; Kim, J.M.; Kim, M.C. An innovative way to measure fatigue crack growth without COD gauge. *Int. J. Fatigue* **2024**, *184*, 108327. [CrossRef]
40. *GB/T 6398-2000*; Standard Test Method for Fatigue Crack Growth Rates of Metallic Materials. China National Standardization Administration (SAC): Beijing, China, 2000. Available online: https://openstd.samr.gov.cn (accessed on 2 January 2025).
41. Tong, L.; Niu, L.; Jing, S.; Ai, L.; Zhao, X.L. Low temperature impact toughness of high strength structural steel. *Thin-Walled Struct.* **2018**, *132*, 410–420. [CrossRef]
42. Wang, S.; Yang, B.; Zhou, S.; Wang, Y.; Xiao, S. Effect of stress ratio and overload on mixed-mode crack propagation behaviour of EA4T steel. *Eng. Fract. Mech.* **2021**, *306*, 110210. [CrossRef]
43. Wang, Y.Q.; Liu, X.Y.; Hu, Z.W.; Shi, Y.J. Experimental study on mechanical properties and fracture toughness of structural thick plate and its butt weld along thickness and at low temperatures. *Fatigue Fract. Eng. Mater. Struct.* **2013**, *36*, 1258–1273. [CrossRef]
44. Kim, K.J.; Lee, J.H.; Park, D.K.; Jung, B.G.; Han, X.; Paik, J.K. An experimental and numerical study on nonlinear impact responses of steel-plated structures in an Arctic environment. *Int. J. Impact Eng.* **2016**, *93*, 99–115. [CrossRef]
45. Qiao, K.; Liu, Z.; Sun, Z.; Wang, X. Effects of low temperature overload and cycling temperature on fatigue crack growth behavior of ship steels in Arctic environments. *Ocean Eng.* **2023**, *288*, 116090. [CrossRef]

Disclaimer/Publisher's Note: The statements, opinions and data contained in all publications are solely those of the individual author(s) and contributor(s) and not of MDPI and/or the editor(s). MDPI and/or the editor(s) disclaim responsibility for any injury to people or property resulting from any ideas, methods, instructions or products referred to in the content.